Received: 11 March 2019 | Revised: 28 May 2019 | Accepted: 21 June 2019

DOI: 10.1002/hbm.24706

RESEARCH ARTICLE

WILEY

A multiparametric analysis of white matter maturation during late childhood and adolescence

Bryce L. Geeraert[1,2] | Robert Marc Lebel[2,3,4] | Catherine Lebel[2,3]

[1]Biomedical Engineering Graduate Program, University of Calgary, Calgary, Alberta, Canada

[2]Alberta Children's Hospital Research Institute and the Hotchkiss Brain Institute, University of Calgary, Calgary, Alberta, Canada

[3]Department of Radiology, University of Calgary, Calgary, Alberta, Canada

[4]GE Healthcare, Calgary, Canada

Correspondence
Catherine Lebel, Department of Radiology, University of Calgary, Calgary, Alberta, Canada.
Email: clebel@ucalgary.ca

Funding information
Canadian Institutes of Health Research; Natural Sciences and Engineering Research Council of Canada

Abstract

White matter development has been well described using diffusion tensor imaging (DTI), but the microstructural processes driving development remain unclear due to methodological limitations. Here, using neurite orientation dispersion and density imaging (NODDI), inhomogeneous magnetization transfer (ihMT), and multicomponent driven equilibrium single-pulse observation of T1/T2 (mcDESPOT), we describe white matter development at the microstructural level in a longitudinal cohort of healthy 6–15 year olds. We evaluated age and gender-related trends in fractional anisotropy (FA), mean diffusivity (MD), neurite density index (NDI), orientation dispersion index (ODI), quantitative ihMT (qihMT), myelin volume fraction (VF_m), and *g*-ratio. We found age-related increases of VF_m in most regions, showing ongoing myelination in vivo during late childhood and adolescence for the first time. No relationship was observed between qihMT and age, suggesting myelin volume increases are driven by increased water content. Age-related increases were observed for NDI, suggesting axonal packing is also occurring during this time. *g*-ratio decreased with age in the uncinate fasciculus, implying changes in communication efficiency are ongoing in this region. FA increased and MD decreased with age in most regions. Gender effects were present in the left cingulum for FA, and an age-by-gender interaction was found for MD in the left uncinate fasciculus. These findings suggest that FA and MD remain useful markers of gender-related processes, and gender differences are likely driven by factors other than myelin. We conclude that white matter development during late childhood and adolescence is driven by a combination of axonal packing and myelin volume increases.

KEYWORDS
brain development, diffusion tensor imaging, magnetic resonance imaging, myelin sheath, white matter

1 | INTRODUCTION

Brain development during childhood and adolescence supports ongoing refinement of behavior and cognitive processes. Postmortem studies of white matter have identified ongoing myelination in adolescence (Benes, 1989; Yakovlev & Lecours, 1967), but are limited by the availability of previously healthy brains and cannot show changes within individuals. Diffusion tensor imaging (DTI) measures have frequently been used to describe trajectories of white matter development, consistently reporting increases of fractional anisotropy (FA) and decreases of mean diffusivity (MD) across childhood and adolescence. These changes are nonlinear, with development slowing and then reaching a plateau sometime during adolescence or early adulthood, depending on the region (Lebel & Beaulieu, 2011; Tamnes, Roalf, Goddings, & Lebel, 2017). Development

in central and posterior white matter tends to reach a plateau sooner than peripheral or anterior structures (Benes, 1989; Simmonds, Hallquist, Asato, & Luna, 2014), and prolonged development of frontotemporal white matter occurs into early adulthood (Lebel, Walker, Leemans, Phillips, & Beaulieu, 2008; Simmonds et al., 2014; Tamnes et al., 2010). While DTI has greatly enhanced our understanding of white matter development, the specific processes underlying this maturation remain unclear.

The uncertainty surrounding white matter development is due, in part, to limitations inherent to DTI. Many factors are important for optimal white matter function, including axon diameter, the density of fibers, myelination, *g*-ratio, and fiber coherence (Figure 1). While DTI measures are sensitive markers of white matter maturity and integrity, they are nonspecific and assess many aspects of white matter microstructure (Beaulieu, 2002). Further, DTI measures are confounded by factors such as crossing or kissing fiber populations, partial volume effects, and processing pipeline biases (Jones, Knosche, & Turner, 2013). Thus, while DTI studies have convincingly shown continued maturation during adolescence, conclusions about specific microstructural processes cannot be made using DTI measures alone.

Recently, measures with increased specificity to individual aspects of white matter microstructure have been used to build upon the foundational DTI literature. Neurite orientation dispersion and density imaging (NODDI) combines multiple diffusion-weighted datasets to construct an advanced diffusion model, and produces indices called neurite density index (NDI) and orientation dispersion index (ODI). NDI is sensitive to intracellular water content, and is an indirect marker of axonal packing in white matter, while ODI assesses the shared orientations of fiber populations in a voxel, and is a marker of tract coherence (Zhang, Schneider, Wheeler-Kingshott, & Alexander, 2012). Inhomogeneous magnetization transfer (ihMT) (Varma, Duhamel, de Bazelaire, & Alsop, 2015) and multicomponent driven equilibrium single-pulse observation of T1/T2 (mcDESPOT) (Deoni, Rutt, Arun, Pierpaoli, & Jones, 2008) leverage the unique magnetic properties of myelin to isolate signal from myelinated tissue, and provide the quantitative ihMT (qihMT) and myelin volume fraction (VF_m) measures, respectively. QihMT and VF_m are correlated and provide improved specificity to myelin over DTI measures (Geeraert et al., 2018). Finally, the *g*-ratio quantifies the ratio of axon diameter to myelin thickness (Stikov et al., 2015), and can be calculated using NDI and VF_m. The *g*-ratio modulates temporal coincidence of signals to a target neuron, and serves as a useful marker of network efficiency, with a theoretical optimal *g*-ratio for transmission speed of approximately 0.6 (Fields, 2008; Rushton, 1951). By combining techniques sensitive to white matter microstructure with DTI, a more complete understanding of white matter developmental trends can be achieved.

While some of these measures have been applied in studies of white matter development, major knowledge gaps remain unexplored. Cross-sectional studies have applied NODDI to show NDI is more sensitive to age-related change than FA or MD (Genc, Malpas, Holland, Beare, & Silk, 2017), and increases during late childhood and adolescence (Chang et al., 2015; Genc, Malpas, et al., 2017; Mah, Geeraert, & Lebel, 2017). On the other hand, ODI undergoes little to no change during childhood and adolescence, suggesting fiber coherence is established early and remains stable during childhood. VF_m studies show rapid myelination in infants and young children (up to 6 years old) following familiar spatial patterns of change (central-to-peripheral, posterior-to-anterior) (Dean et al., 2016; Deoni, Dean, O'Muircheartaigh, Dirks, & Jerskey, 2012). These studies also suggest that myelination occurs earlier in females (Dean et al., 2015), but VF_m has not been applied to investigate late childhood or adolescent development. Only one small study (n = 18) examined age-related changes in *g*-ratio, showing decreases in multiple brain regions from birth to ~7.5 years (Dean et al., 2016). Typical magnetization transfer (MT) techniques have shown minimal change in magnetization transfer ratio during childhood and adolescence (Moura et al., 2016;

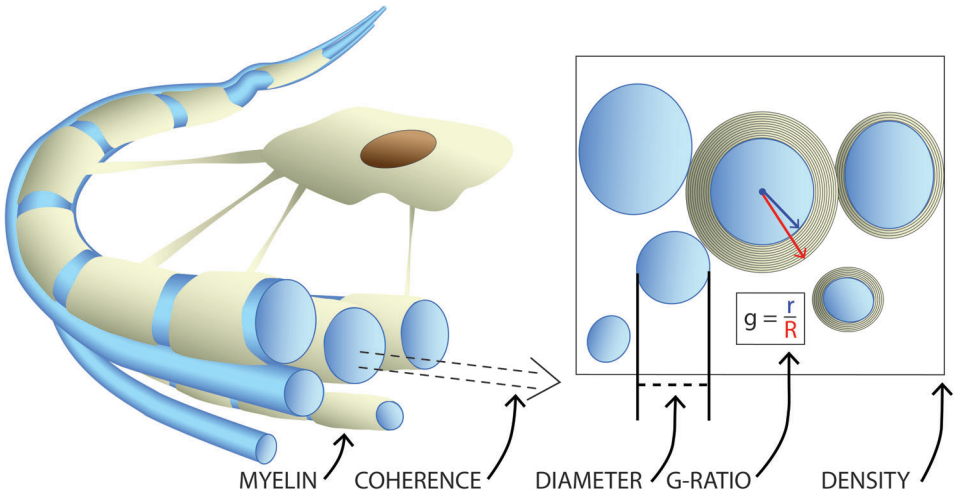

FIGURE 1 Important microstructural factors in a bundle of axons (blue). At the individual level, axon diameter and myelin thickness influence the speed of action potential propagation along the axon. The *g*-ratio combines these factors to describe conduction efficiency of a fiber. The coherence of fibers, along with the density or packing of axons in a region, are additional factors influencing the effectiveness of information transfer along groups of white matter fibers, often grouped into major tracts based upon their shared termination points [Color figure can be viewed at wileyonlinelibrary.com]

Pangelinan et al., 2016; Perrin et al., 2009), but no study has yet implemented ihMT to evaluate myelin in development.

This study sought to describe white matter development during late childhood and adolescence in new detail. DTI, NODDI, ihMT, and mcDESPOT scans were collected to produce FA, MD, NDI, ODI, qihMT, VF_m, and *g*-ratio in a longitudinal sample. Through this combination of white matter structural and microstructural measures, a multifaceted assessment of white matter development during late childhood and adolescence can be achieved. We applied these techniques both globally and within individual white matter tracts to describe overall developmental trends and compare our findings to previous diffusion-based literature. Based on extensive previous work, we expected to see increases in FA and NDI, decreases in MD, and no change in ODI. The examination of VFm, qihMT, and *g*-ratio trends was novel, and performed in an exploratory manner.

2 | METHODS

2.1 | Subjects

This study included 73 datasets on 50 healthy children aged 6–15 years (28 males/22 females) who were recruited as part of an ongoing study on adolescent brain development. Children were recruited between 6 and 13 years of age (10.3 ± 2.4 years); 23 children (10 males/13 females, mean: 13.5 ± 2.1 years) returned 2 years after their initial visit for a second scan. Inclusion criteria were: (a) uncomplicated birth between 37 and 42 weeks' gestation, (b) no history of developmental disorder or psychiatric disease, (c) no history of neurosurgery, and (d) no contraindications to MRI. All subjects provided informed assent and parents/guardians provided written informed consent. This study was approved by the local research ethics board (ethics ID: REB13-1346). Three subjects of an initial 53 were excluded due to unacceptable motion corruption in their diffusion-weighted datasets.

2.2 | Image acquisition

Subjects were scanned using a 32-channel head coil on a GE 3T Discovery MR750w (GE, Milwaukee, WI) system at the Alberta Children's Hospital. Two diffusion-weighted datasets were acquired at b = 900 s/mm^2 and 2,000 s/mm^2 using a spin-echo echo planar imaging sequence with TR/TE = 12 s/88 ms, 2.2 mm × 2.2 mm × 2.2 mm resolution, with 5 b = 0 s/mm^2 volumes and 30 gradient directions per volume, scan duration = 14:24 min. IhMT images used a 3D SPGR sequence: TR/TE = 10.46 ms/2.18 ms, 2.2 mm × 2.2 mm × 2.2 mm resolution, flip angle 8°, scan time 5:12 min. The sequence included a 5 ms Fermi pulse with peak B1 of 45 mG and 5 kHz offset prior to each excitation. The MT condition cycled between positive offset (+5 kHz), dual offset (±5 kHz), negative offset (−5 kHz), and dual offset. A 32° flip angle reference image with no MT pulse was acquired for quantification. For mcDESPOT, multiflip angle 3D SPGR images (α = 3°, 4°, 5°, 6°, 7°, 9°, 13°, and 18°) were collected with TR/TE = 9.1 ms/3.9 ms, 1.7 mm × 0.86 mm × 1.7 mm resolution; IR-SPGR images were collected to correct for B_1 inhomogeneity using 5° α, TR/TE = 9.1 ms/3.9 ms, 2.29 mm × 0.86 mm × 3.4 mm resolution; two multiflip angle bSSFP images were collected at phase 0° and 180° to correct for B_0 inhomogeneity, with α = 10°, 13°, 16°, 20°, 23°, 30°, 43°, and 60°, TR/TE = 6.6 ms/3.2 ms, 1.7 mm × 0.86 mm × 1.7 mm resolution. Total scan time for mcDESPOT was 16:35 min. T1-weighted anatomical images were acquired to use for anatomical reference, with TI = 600 ms, TR/TE = 8.2 ms/3.2 ms, 0.8 mm × 0.8 mm × 0.8 mm resolution, scan duration 5:38. Due to time limitations and poor data quality as a result of subject motion, not all datasets were available for all participants. Our final dataset for analysis consisted of 73 DTI datasets (50 children), 71 NODDI datasets (48 children), 71 qihMT datasets (48 children), 59 mcDESPOT datasets (37 children), and 54 *g*-ratio datasets (37 children).

2.3 | Image processing

All images were visually inspected for quality assessment and processed separately using appropriate tools before being combined for further analysis. T1 images were processed through FreeSurfer 5.3 (http://surfer.nmr.mgh.harvard.edu/) for intensity normalization and brain extraction. ExploreDTI (Leemans, Jeurissen, Sijbers, & Jones, 2009) was used to preprocess DTI datasets, including signal drift correction, brain extraction, eddy current and motion corrections, and registration to post-FreeSurfer T1 images for correction of geometric distortions induced by echo-planar imaging. The REKINDLE model was used in ExploreDTI to produce FA and MD maps for each subject (Tax, Otte, Viergever, Dijkhuizen, & Leemans, 2015). ExploreDTI's semiautomated tractography tool was used to segment the corpus callosum splenium, body, and genu, and the corticospinal tract (CST), cingulum, arcuate, inferior frontooccipital (IFOF), inferior longitudinal (ILF), and uncinate fasciculi, bilaterally (Figure 2, subplot F). An 11-year old female with typical data quality (showcased in Figure 2) was selected as the exemplar participant for this process; all regions were drawn on this template brain and then registered to other participants' data for tracking in native space (Lebel, Rasmussen, et al., 2008). DTI data was exported to the NODDI Matlab Toolbox (http://www.nitrc.org/projects/noddi_toolbox) for calculation of isotropic (f_{iso}) and intracellular (f_{icvf}, or NDI) volume fractions and ODI.

Pseudoquantitative ihMT maps (qihMT) were obtained from ihMT data using an in-house GE protocol, and were derived from the following equation, assuming R1TR << 1, and α << 1 rad:

$$\text{qihMT} \equiv (R1_{\text{dual}} - R1_{\pm}) \cong \frac{c\alpha^2}{2TR} S_c \left(\frac{1}{S_{\text{dual}}} - \frac{1}{S_{\pm}} \right)$$

where $R1$ is the average longitudinal relaxation rate from repetitions of an MT state (either dual frequency or single frequency), S is the signal measured during this MT state, c = 4 is a flip angle scale factor between the excitation angle of the MT and reference conditions, α is the nominal flip angle, and S_c is signal from our 32° flip angle reference state. qihMT is approximated by $\Delta(R1)$ and describes the difference in longitudinal relaxation rates between these two states. Compared to magnetization transfer ratio (MTR), this qihMT formulation offers a simple yet robust

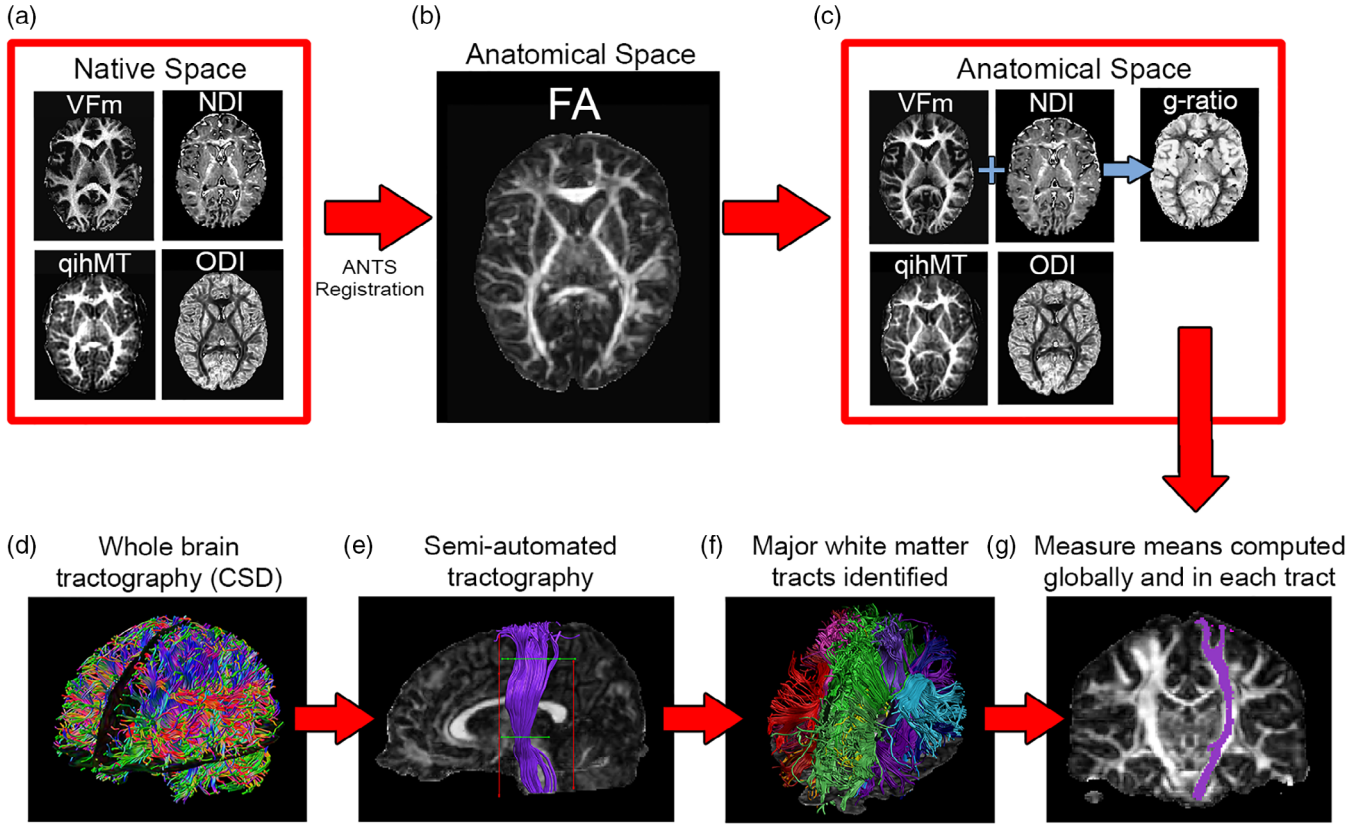

FIGURE 2 Following data quality assessment and preprocessing, native space neurite density index (NDI), orientation dispersion index (ODI), myelin volume fraction (VF_m), and quantitative ihMT (qihMT) maps (a) were normalized to subject fractional anisotropy (FA) maps in T1 space (b), resulting in anatomically relevant measure maps and allowing *g*-ratio computation (c). Meanwhile, whole-brain tractography via constrained spherical deconvolution (CSD) (d) and semiautomated tractography (e) was conducted in ExploreDTI to identify major white matter tracts in each participant's brain (f). Finally, mean FA, mean diffusivity (MD), NDI, ODI, qihMT, VF_m, and *g*-ratio were calculated globally and by averaging across voxels in each tract (g) [Color figure can be viewed at wileyonlinelibrary.com]

metric by reducing sensitivity to T1 and B1 inhomogeneity. This formulation is based on the methods of Helms, Dathe, Kallenberg, and Dechent (2008) and Zaiss et al. (2014). Following qihMT production, brain extraction was performed for qihMT images using FSL's BET2 tool (Smith, 2002).

mcDESPOT SPGR, IR-SPGR, and bSSFP images were aligned to the SPGR image with the largest α, then processed by fitting T1, T2, and volume fractions to three water compartments (myelin-bound, intra/extracellular, and free), along with exchange rates between myelin-bound and intra/extracellular water (Deoni, Matthews, & Kolind, 2013). The myelin-bound water volume fraction from this fitting was used to produce VF_m maps for each participant. *g*-ratio maps were computed using VF_m, NDI, and f_{iso} maps to calculate the fiber volume fraction (FVF) and *g*-ratio using the following two equations:

$$FVF = VF_m + (1 - VF_m)(1 - f_{iso})NDI$$

$$g - ratio = \sqrt{(1 - VF_m)/FVF}$$

Following production of all measure maps, qihMT, VF_m, NDI, and ODI maps were registered to b = 900 s/mm^2 FA maps using Advanced Normalization Tools (ANTs) (Avants et al., 2011). Default parameters from antsRegistrationSyN.sh were used, with the –t s flag chosen to select rigid, affine, and deformable symmetric normalization transforms. Measure means were calculated globally from a brain mask computed by ExploreDTI, and for each tract per participant. Figure 2 summarizes how images were combined for multimodal assessment of white matter microstructure.

2.4 | Statistical analysis

Linear mixed effects models were computed in MATLAB R2015a (Mathworks, Natick, MA) for each measure and region of interest (global mask and specific tracts). No scaling was applied to measures before model computation. All available time point 1 and time point 2 data was included in these models. Models included subject age, gender, and age-by-gender interaction as fixed effects, and a random intercept was included for each subject. Both linear and quadratic age terms were included in the model. Models were fit using maximum likelihood estimation. An example model formula is presented below.

$$FA \sim Age^2 + Age + Gender + Age{*}Gender + (1|Subject)$$

Reduced models without quadratic age effects and age-by-gender interactions were also evaluated, resulting in four models computed

per region—full model, quadratic age term removed, age-by-gender interaction term removed, and quadratic age and age-by-gender interaction terms removed. The Bayesian Information Criterion (BIC) was used to determine which of these four models best explained our data, with lower BIC reflecting better fit for our data. Bayes factors were also computed to assess statistical power, to supplement findings generate via null hypothesis testing (Kass & Raftery, 1995). A Bayes factor less than 1/3 was considered evidence for the null hypothesis, between 1/3 and 3 was considered evidence of low power, while Bayes factors of greater than 3 were considered evidence for the alternative hypothesis. False discovery rate (FDR) corrections were applied via the Benjamini-Hochberg method to account for 105 comparisons for each measure across tracts, with overall significance set to $q = 0.05$ (Benjamini & Hochberg, 1995). Age, quadratic age, and gender findings were corrected separately. A follow-up analysis was also conducted using the more stringent Benjamini-Yekutieli FDR correction (Benjamini & Yekutieli, 2001).

3 | RESULTS

3.1 | Predictive factors from linear mixed effects models

Mean and standard deviation for all measures in each region at each time point are presented in Table 1. Globally, age was a significant predictor for FA ($t = 4.84$, $p < .001$), MD ($t = -3.03$, $p = .0035$), NDI ($t = 3.05$, $p = .0033$), and VF_m ($t = 2.91$, $p = .0054$), but not qihMT, ODI, or *g*-ratio. Gender was not predictive of any measure in global models. Additionally, quadratic models outperformed linear models for both MD (age^2 $t = 3.26$, $p = .0018$) and NDI (age^2 $t = -2.53$, $p = .014$). MD decreases and NDI increases became more gradual with age.

Statistics from linear mixed effects models within tracts are summarized quantitatively in Table 2. Significant effects, which survived FDR corrections, are marked by an asterisk (*). Age was found to be predictive of FA, MD, NDI, and VF_m in many tracts. FA, MD, and NDI changed more in magnitude than VF_m, except in the uncinate fasciculus. A main effect of gender was identified for FA in the left cingulum, such that boys had higher FA than girls. A significant interaction between age and gender was found for MD in the left uncinate fasciculus ($t = -2.57$, $p = .012$). Follow up mixed models regressions were run to identify age was related to decreases in MD for males ($t = -4.58$, $p < .001$), but no significant relationship with age was observed in girls ($t = 0.71$, $p = .48$). Clusters of tracts developing similarly are described by Figure 3, while Figure 4 demonstrates the age*gender interaction found for MD in the left uncinate fasciculus. Model degrees of freedom, adjusted R^2, along with parameter estimates and standard deviations for all effects included in models are provided in Table S1, while confidence intervals for parameter estimates are provided in Table S2. Parameters from follow-up linear mixed effects models conducted to investigate the age*gender interaction present in the left uncinate for MD are summarized in Table S3.

As a follow-up analysis, we also examined our results after performing FDR corrections via the Benjamini-Yekutieli method (Benjamini & Yekutieli, 2001) for 105 comparisons, to account for the dependence of results from our measures. When corrections were applied in this fashion, age effects were no longer significant ($q < 0.05$) for FA in the left ILF and right uncinate, for MD in the left ILF, left uncinate, right cingulum, right CST, and genu, for NDI in the left arcuate and bilateral cingulum and uncinate, for MWF in the left ILF, bilateral IFOF, cingulum, left CST, and corpus callosum, and for *g*-ratio in the left uncinate. No gender effects survived this correction method.

3.2 | Linear and quadratic age effects

For most tracts, models with only linear age effects were superior to models including both quadratic and linear age effects ($BIC_{quadratic} - BIC_{linear}$ range: 0.16–5.76). However, models including quadratic age effects provided superior fits for MD in the splenium and for NDI in all regions except the right IFOF, right CST, and splenium (Table 2). Bayes factors were computed to compare the fit of quadratic models vs reduced models with linear age effects only. This analysis suggested that absence of quadratic age effects may be due to low power in the right IFOF ($BF_{inclusion} = 0.94$) and splenium ($BF_{inclusion} = 1.22$), and suggested that a quadratic age effect is absent in the right CST ($BF_{inclusion} = 0.26$). In all regions where models including quadratic age effects were superior, quadratic age effects did not remain significant following multiple comparison corrections. Rates of change decreased (i.e., became more gradual) with age in all models where quadratic fits were superior.

4 | DISCUSSION

Here, we describe trends in myelin water fraction during adolescence for the first time. Together with our NDI, FA, and MD findings, these suggest that most tracts are undergoing both myelination and increases of axonal packing during late childhood and adolescence. Major white matter tracts can be classified by their developmental patterns, resulting in three clusters of major white matter tracts developing similarly. A cluster of right hemisphere tracts (Figure 3, subplot A) showed age-related increases in NDI, suggesting development driven by changes in axonal packing. A widespread network of commissural, projection, and association tracts (Figure 3, subplot B) showed age effects for VF_m alongside NDI in childhood and adolescence, suggesting ongoing myelination and increased axon packing. *g*-ratio changes accompanied VF_m and NDI changes in the left uncinate fasciculus (Figure 3, subplot C), suggesting additional changes in communication efficiency within these frontotemporal connections. These findings add specificity to previous studies of white matter development during childhood and adolescence, and shed new light on how brain development may link to cognitive and behavioral maturation across adolescence.

Myelin volume fraction (VF_m) increased with age in many white matter tracts. VF_m provides increased specificity to myelin over DTI,

TABLE 1 Mean and standard deviation for measures of white matter microstructure in major white matter tracts throughout the brain. Visit 1 data was collected from the visits of 50 children aged 6–15, while visit 2 data consists of 23 data points from children who have returned for a follow-up visit, 2 years after their initial scan

Region	Visit	VF_m	qihMT	*g*-ratio	NDI	ODI	FA	MD
Global	1	0.08 ± 0.01	46.6 ± 8.3	0.91 ± 0.01	0.46 ± 0.03	0.41 ± 0.02	0.23 ± 0.01	1.0E−3 ± 5.2E−5
	2	0.09 ± 0.01	43.8 ± 7.0	0.91 ± 0.01	0.46 ± 0.03	0.41 ± 0.02	0.23 ± 0.01	1.0E−3 ± 6.3E−5
L AF	1	0.14 ± 0.02	83.4 ± 14.5	0.87 ± 0.02	0.54 ± 0.05	0.29 ± 0.03	0.39 ± 0.02	8.3E−4 ± 2.9E−5
	2	0.15 ± 0.02	87.3 ± 11.7	0.87 ± 0.01	0.55 ± 0.05	0.29 ± 0.03	0.40 ± 0.02	8.1E−4 ± 2.4E−5
R AF	1	0.14 ± 0.02	83.4 ± 14.8	0.87 ± 0.02	0.53 ± 0.04	0.28 ± 0.02	0.40 ± 0.02	8.1E−4 ± 3.3E−5
	2	0.15 ± 0.02	84.1 ± 11.1	0.87 ± 0.01	0.54 ± 0.04	0.29 ± 0.02	0.41 ± 0.01	7.9E−4 ± 3.0E−5
L ILF	1	0.14 ± 0.02	81.2 ± 10.2	0.86 ± 0.02	0.50 ± 0.04	0.27 ± 0.02	0.39 ± 0.02	8.6E−4 ± 3.0E−5
	2	0.14 ± 0.01	82.4 ± 9.8	0.86 ± 0.01	0.50 ± 0.04	0.27 ± 0.02	0.40 ± 0.02	8.6E−4 ± 3.3E−5
R ILF	1	0.13 ± 0.02	76.1 ± 14.7	0.87 ± 0.02	0.49 ± 0.03	0.28 ± 0.03	0.38 ± 0.03	8.6E−4 ± 3.0E−5
	2	0.12 ± 0.02	74.6 ± 12.7	0.88 ± 0.02	0.49 ± 0.04	0.29 ± 0.04	0.38 ± 0.04	8.5E−4 ± 2.3E−5
L IFOF	1	0.14 ± 0.02	80.0 ± 12.5	0.87 ± 0.02	0.50 ± 0.03	0.26 ± 0.02	0.41 ± 0.02	8.7E−4 ± 2.6E−5
	2	0.14 ± 0.01	84.2 ± 9.3	0.86 ± 0.01	0.50 ± 0.03	0.25 ± 0.02	0.41 ± 0.01	8.6E−4 ± 2.0E−5
R IFOF	1	0.13 ± 0.02	80.0 ± 12.5	0.87 ± 0.02	0.45 ± 0.04	0.28 ± 0.04	0.35 ± 0.02	9.2E−4 ± 3.0E−5
	2	0.14 ± 0.01	78.3 ± 9.5	0.87 ± 0.01	0.50 ± 0.04	0.26 ± 0.02	0.42 ± 0.02	8.4E−4 ± 2.6E−5
L UF	1	0.12 ± 0.02	79.2 ± 16.1	0.87 ± 0.03	0.45 ± 0.04	0.28 ± 0.04	0.35 ± 0.02	9.2E−4 ± 3.0E−5
	2	0.13 ± 0.02	79.0 ± 12.9	0.86 ± 0.01	0.45 ± 0.03	0.28 ± 0.04	0.35 ± 0.03	9.1E−4 ± 4.4E−5
R UF	1	0.12 ± 0.02	73.9 ± 16.2	0.87 ± 0.02	0.46 ± 0.04	0.27 ± 0.03	0.36 ± 0.02	8.9E−4 ± 3.6E−5
	2	0.12 ± 0.01	70.5 ± 15.5	0.87 ± 0.01	0.46 ± 0.03	0.27 ± 0.03	0.36 ± 0.02	8.8E−4 ± 3.2E−5
L CING	1	0.11 ± 0.02	63.9 ± 12.4	0.90 ± 0.02	0.48 ± 0.04	0.32 ± 0.03	0.33 ± 0.02	8.9E−4 ± 4.2E−5
	2	0.11 ± 0.01	61.8 ± 6.2	0.89 ± 0.01	0.49 ± 0.04	0.32 ± 0.03	0.34 ± 0.02	8.7E−4 ± 2.6E−5
R CING	1	0.11 ± 0.02	64.5 ± 14.8	0.89 ± 0.02	0.49 ± 0.04	0.32 ± 0.03	0.33 ± 0.03	8.6E−4 ± 2.8E−5
	2	0.11 ± 0.01	59.1 ± 8.5	0.90 ± 0.01	0.49 ± 0.03	0.32 ± 0.03	0.34 ± 0.03	8.5E−4 ± 2.2E−5
L CST	1	0.14 ± 0.01	93.4 ± 15.9	0.87 ± 0.01	0.56 ± 0.05	0.24 ± 0.02	0.45 ± 0.03	8.6E−4 ± 7.2E−5
	2	0.15 ± 0.01	92.9 ± 12.0	0.87 ± 0.01	0.57 ± 0.03	0.23 ± 0.02	0.46 ± 0.03	8.6E−4 ± 6.1E−5
R CST	1	0.14 ± 0.02	98.2 ± 18.4	0.87 ± 0.01	0.56 ± 0.04	0.23 ± 0.03	0.47 ± 0.04	8.3E−4 ± 5.0E−5
	2	0.15 ± 0.02	95.7 ± 12.9	0.88 ± 0.01	0.57 ± 0.04	0.23 ± 0.03	0.48 ± 0.04	8.3E−4 ± 6.9E−5
Genu	1	0.15 ± 0.02	85.0 ± 15.1	0.85 ± 0.02	0.50 ± 0.04	0.25 ± 0.03	0.41 ± 0.02	9.4E−4 ± 3.8E−5
	2	0.15 ± 0.01	73.6 ± 10.2	0.85 ± 0.01	0.49 ± 0.04	0.25 ± 0.03	0.41 ± 0.01	9.3E−4 ± 2.9E−5
Body	1	0.12 ± 0.02	73.5 ± 12.0	0.87 ± 0.02	0.50 ± 0.03	0.28 ± 0.03	0.37 ± 0.03	9.6E−4 ± 4.3E−5
	2	0.13 ± 0.01	70.0 ± 8.4	0.88 ± 0.01	0.50 ± 0.03	0.29 ± 0.03	0.37 ± 0.03	9.5E−4 ± 4.8E−5
Splenium	1	0.13 ± 0.02	75.0 ± 11.2	0.87 ± 0.02	0.52 ± 0.04	0.26 ± 0.02	0.41 ± 0.03	9.3E−4 ± 4.1E−5
	2	0.13 ± 0.01	75.4 ± 8.8	0.87 ± 0.01	0.52 ± 0.04	0.26 ± 0.03	0.43 ± 0.02	9.3E−4 ± 4.2E−5

and is sensitive to age-related processes in myelin in our sample. VF_m's sensitivity to myelin has been validated histologically in healthy and cuprizone-treated mice (Wood et al., 2016) and the shaking pup model (Hurley et al., 2010), along with in vivo studies of multiple sclerosis (Kolind et al., 2012; Kolind et al., 2015), and it shows good reproducibility within and across sites (Laule & Moore, 2018). Previous imaging studies using the same measure have shown rapid myelination during infancy (Deoni et al., 2011; Deoni et al., 2012), and histological studies have shown continued myelination into adolescence (Benes, 1989; Yakovlev & Lecours, 1967), but this is the first study to demonstrate VF_m trends in late childhood and adolescence, and the first to show ongoing myelination in vivo. Rates of age-related change in VF_m varied regionally, with the arcuate and uncinate appearing to have the largest changes. These tracts are among the latest to plateau for FA and MD, showing continued development into young adulthood (Lebel & Beaulieu, 2011; Simmonds et al., 2014). Interestingly, a network of right hemisphere tracts—the cingulum, arcuate, ILF, and CST—showed age effects for NDI and FA, but did not show effects in VF_m. More findings of VF_m increases in the left hemisphere than the right may indicate leftward asymmetry of white matter development during adolescence. Leftward asymmetry in rates of change have been reported previously in diffusion studies of development for many regions (Krogsrud et al., 2016), but further research is needed to investigate this possibility.

TABLE 2

	Tract		VF_m	qihMT	*g*-ratio	NDI	ODI	FA	MD
L	AF	Age	3.23*	−0.04	−0.26	5.71*	0.52	4.40*	−5.32*
		Age^2				−2.37			
		Gender	0.69	1.40	−1.12	−0.83	−0.26	1.91	1.07
R	AF	Age	1.88	0.50	0.79	3.87*	0.78	3.63*	−5.63*
		Age^2				−3.15			
		Gender	−0.11	−0.51	1.40	0.48	1.24	−0.16	1.40
L	ILF	Age	2.75*	−0.56	−0.67	3.26*	1.28	2.82*	−2.80*
		Age^2				2.65		−2.42	
		Gender	1.07	1.44	−0.92	0.04	−0.44	2.00	−0.88
R	ILF	Age	1.71	−0.17	−0.13	3.14*	0.61	1.50	−4.50*
		Age^2				−2.46			
		Gender	0.65	0.50	−0.82	0.47	−0.16	1.02	0.24
L	IFOF	Age	2.87*	0.32	−1.29	3.47*	−0.60	4.48*	−3.20*
		Age^2				−2.90			
		Gender	0.86	1.39	−0.78	0.09	0.39	2.27	−1.37
R	IFOF	Age	2.79*	−0.67	−0.53	5.76*	−0.95	6.09*	−4.44*
		Gender	0.36	0.34	−0.81	−0.24	0.17	1.09	−0.42
L	UF	Age	3.66*	−0.45	−3.11*	2.79*	0.12	1.49	0.87*
		Age^2				−2.51			
		Gender	2.26	1.90	−1.60	0.36	0.24	2.57	−1.93
		Age*gender							−2.57*
R	UF	Age	3.29*	−1.64	−2.68*	2.68*	0.40	2.59*	−0.50
		Age^2	−2.94		2.47	−2.30			
		Gender	1.44	0.90	−1.27	1.50	0.40	3.11	2.04
		Age*gender							−2.14
L	CING	Age	2.69*	−0.30	−0.76	2.92*	0.49	1.23	−1.24
		Age^2				−2.49			
		Gender	1.55	1.47	−1.09	0.22	−1.26	3.99*	−0.54
R	CING	Age	2.05	−0.95	−0.19	2.94*	1.75	1.59	−2.96*
		Age^2				−2.46			
		Gender	1.42	0.93	−1.26	1.24	−1.43	2.64	0.27
L	CST	Age	2.38*	0.52	0.62	3.42*	−1.59	3.85*	−1.95
		Age^2				−2.50			
		Gender	−0.40	0.18	0.80	−0.11	1.75	−1.13	1.64
R	CST	Age	1.68	0.58	1.33	7.08*	−1.19	3.85*	−2.76*
		Gender	−0.27	−0.37	0.65	−0.04	1.86	−1.50	1.51
	Genu	Age	2.48*	−2.87	−1.03	3.53*	0.84	1.15	−2.97*
		Age^2				−3.15			
		Gender	1.58	1.23	−1.17	0.70	0.70	2.14	−0.06
	Body	Age	2.72*	0.09	−0.60	3.52*	−1.39	5.66*	−1.62
		Age^2				−2.83			
		Gender	0.31	0.82	−0.65	−0.18	0.75	0.30	0.57
	Splenium	Age	2.54*	0.65	−0.36	6.43*	−1.28	6.68*	−3.93*
		Age^2							3.63
		Gender	0.26	0.87	−0.51	−0.22	−0.09	1.43	0.02

While age effects were significant for VF_m in a widespread network of white matter tracts, no age effects were observed for qihMT in our sample. QihMT is correlated with VF_m (Geeraert et al., 2018), but these measures assess myelin through different methods. The mcDESPOT model estimates the fraction of water bound within the myelin sheath based on the unique T1 and T2 characteristics of water in that environment (Deoni et al., 2008), while ihMT provides contrast based upon dipolar coupling in lipid bilayers, and is primarily driven by

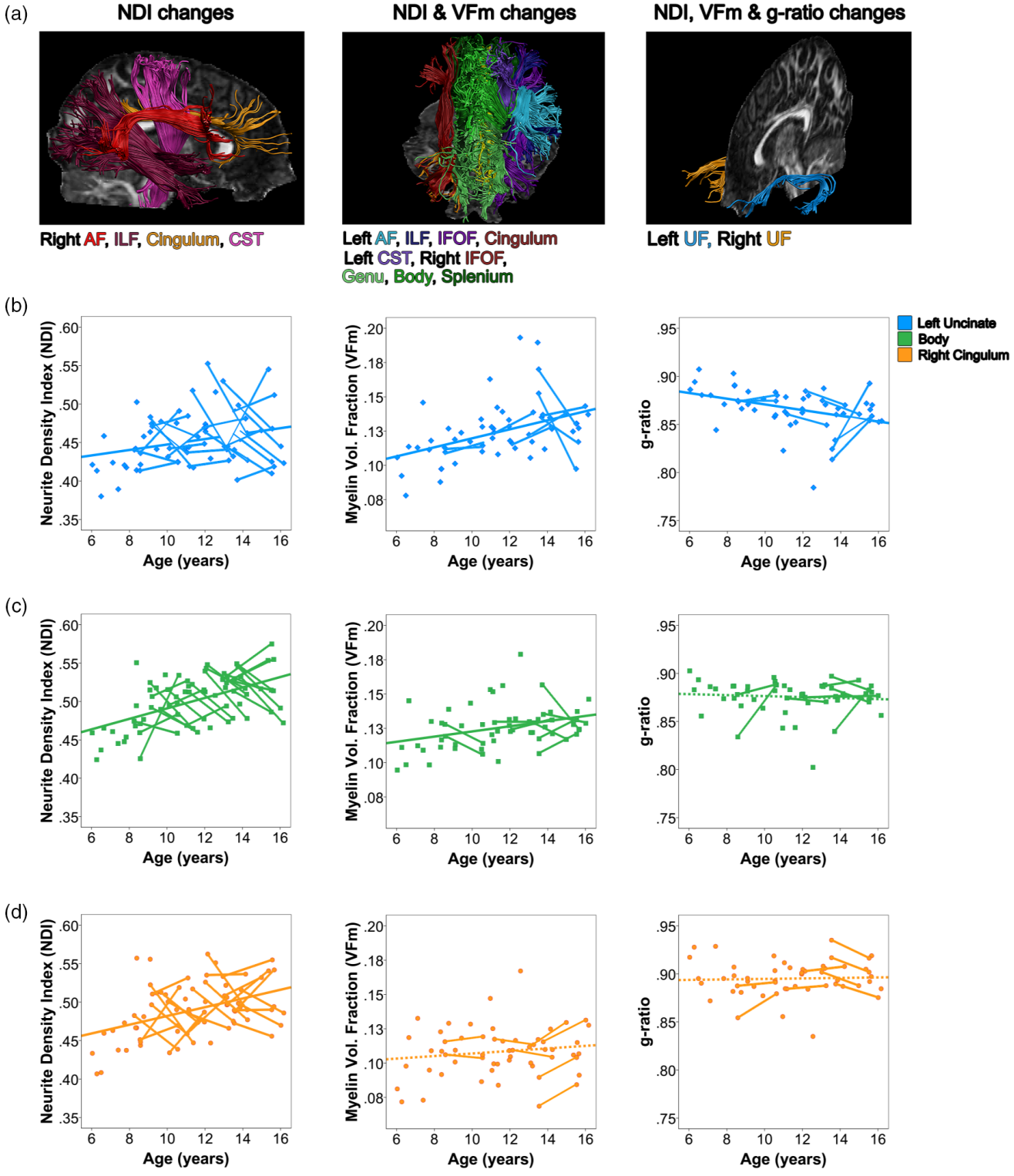

FIGURE 3 Developmental processes in white matter microstructure during childhood and adolescence. Major white matter tracts can be grouped into three clusters with similar developmental profiles, visualized in Panel (a). Scatterplots from the left uncinate fasciculus (b), corpus callosum body (c), and right cingulum (d) are displayed to demonstrate trends in neurite density index (NDI), myelin volume fraction (VF_m), and *g*-ratio for each cluster of tracts developing similarly [Color figure can be viewed at wileyonlinelibrary.com]

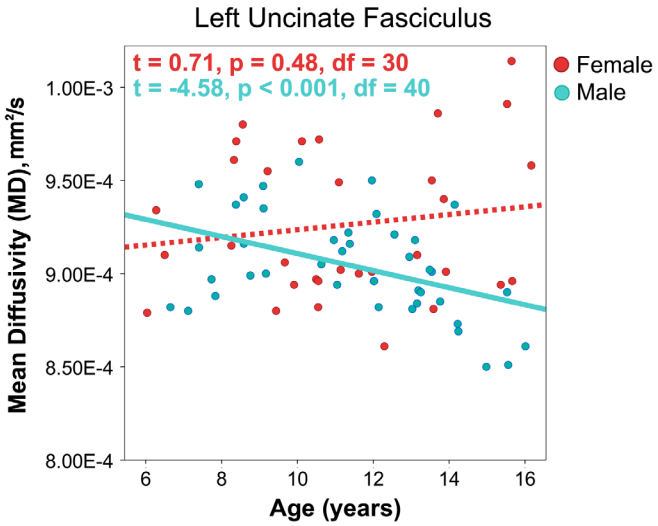

FIGURE 4 An interaction between age and gender was present for MD in the left uncinate fasciculus, such that males showed anticipated age-related decreases in MD, but no significant relationship was observed in females. *T* statistics for age effects are reported from follow up mixed effects models regressions to investigate relationships within males and females separately [Color figure can be viewed at wileyonlinelibrary.com]

myelin in white matter tissue (Manning, Chang, MacKay, & Michal, 2017; Prevost et al., 2017; Swanson et al., 2017). While no other studies have used ihMT to probe white matter development, previous MT studies have found slight decreases or no change in MTR during adolescence (Moura et al., 2016; Pangelinan et al., 2016; Perrin et al., 2009). MTR probes general macromolecular content (Berry et al., 1999; Schmierer, Scaravilli, Altmann, Barker, & Miller, 2004; Stanisz, Webb, Munro, Pun, & Midha, 2004), so these studies are less specific to myelin than our ihMT findings. Still, these findings align with our ihMT results, and imply that myelin content is stable during adolescence. However, we cannot dismiss the possibility that MT/ihMT studies to date lack the statistical power to detect changes in myelin content that are occurring during this period. Histological research has revealed that myelination continues throughout adolescence (Benes, 1989; Yakovlev & Lecours, 1967), thus it remains possible that MT and ihMT measures applied to date have lacked the sensitivity required to describe myelination during this period. Optimizations to ihMT methods have been identified which may enable future studies to address myelination trajectories during adolescence with greater clarity (McHinda et al., 2018; Prevost et al., 2017). When considered together, our VF_m and qihMT findings suggest that myelin sheaths may be incorporating more water between a relatively stable number of wrapped membranes during adolescence. Inclusion of ihMT measures alongside the myelin volume fraction provides a multifaceted assessment of myelin volume fraction, and implies fascinating nuance in myelination during late childhood and adolescence.

Increases in fiber volume fraction, as assessed by NDI, and myelin volume fraction were found in most regions, but age effects were found for the *g*-ratio in the left and right uncinate fasciculi. Developmentally, *g*-ratio decreases in infancy (Dean et al., 2016), suggesting increasing myelin thickness relative to axon diameter. Our results imply that during late childhood and adolescence, NDI and VF_m increase at similar rates in most tracts, resulting in negligible change in the ratio between axon diameter and myelin thickness except in the bilateral uncinate fasciculus. Significant age-related decreases of *g*-ratio in the uncinate fasciculi are likely driven by smaller increases in NDI and greater increases in VF_m compared to other regions, as displayed in Figure 3. The uncinate fasciculus is known to be among the latest-developing tracts (Lebel, Walker, et al., 2008), thus the *g*-ratio may reach a developmental plateau earlier than other measures still showing age-related increases in our sample, leaving only frontotemporal connections showing ongoing change.

Age-related changes in diffusion-based measures were expected and agree well with previous findings. FA increased with age in all regions except the right ILF, left uncinate, bilateral cingulum, and genu. MD decreased linearly with age in most regions, but no age effect was observed in the left cingulum, CST, and body. Our findings reflect the regional variation in developmental timing established by previous studies (Giorgio et al., 2010; Krogsrud et al., 2016; Lebel & Beaulieu, 2011; Simmonds et al., 2014). NODDI measures help to clarify trends in DTI measures, and have been leveraged by previous cross-sectional studies to describe age-related trends in white matter with greater specificity. Our longitudinal results are in line with previous cross-sectional findings of positive correlations between NDI and age and no correlation with ODI during adolescence (Chang et al., 2015; Genc, Malpas, et al., 2017; Mah et al., 2017). While most regions and measures showed linear trends, quadratic models outperformed linear models for MD in the splenium, and NDI in all regions except the right IFOF, right CST, and splenium, however, quadratic age effects did not survive multiple comparisons. When viewed across the full developmental period, white matter maturation is nonlinear (Lebel, Treit, & Beaulieu, 2017), but can appear linear when considering restricted age ranges. NDI has previously been shown to be more sensitive to age-related change than diffusion measures (Genc, Malpas, et al., 2017), thus NDI may be sensitive enough to developmental processes to appropriately describe nonlinear white matter development occurring during adolescence. In regions where quadratic models outperformed linear models, rates of change decreased with age, and measures were likely approaching their developmental plateau.

Gender effects were found for FA bilaterally in the uncinate and in the left cingulum. In all cases, FA was higher for males than females. Previous investigations of gender differences have been mixed, and many studies have identified no significant FA or MD differences between males and females (Bonekamp et al., 2007; Eluvathingal, Hasan, Kramer, Fletcher, & Ewing-Cobbs, 2007; Giorgio et al., 2010; Uda et al., 2015), while other studies report significant gender differences in some brain regions, with inconsistent location and direction of differences (for review, see [Geeraert, Reynolds, & Lebel, in press; Lebel et al., 2017]). We also found an age-by-gender interaction for MD in the left uncinate such that MD decreased with age in boys but no relationship was observed in girls, as shown in Figure 4. A similar interaction was found in the right uncinate, but this finding did not survive FDR correction.

We performed a Bayes factor analysis to determine whether these interactions were exclusive to MD or may also be present for other

measures which showed age effects, namely FA, NDI, and VF_m. This analysis implied an absence of age-by-gender interactions for VF_m (Left: $BF_{inclusion}$ = 0.14; Right: $BF_{inclusion}$ = 0.21) and NDI (Left: $BF_{inclusion}$ = 0.11; Right: $BF_{inclusion}$ = 0.11). However, Bayes factors for FA in the uncinate fasciculus implied that absence of an age-by-gender interaction in the left uncinate could be due to low power ($BF_{inclusion}$ = 2.32) and was likely present for the right uncinate ($BF_{inclusion}$ = 4.8). This suggests that diffusion measures may provide capture information regarding gender differences that is not captured by more specific measures, such as VF_m and NDI. Like the findings of absolute differences in diffusion parameters, previous research in this age range shows mixed results, with some studies showing no differences in trajectories between males and females (Krogsrud et al., 2016; Muftuler et al., 2012), while others show FA increases for males but not females (Simmonds et al., 2014), and later FA plateaus in males (Chen, Zhang, Yushkevich, Liu, & Beaulieu, 2016). While gender effects on development remain unclear, our findings support the hypothesis of distinct developmental trajectories between males and females. The presence of FA gender differences in the absence of VF_m or qihMT differences may indicate that gender differences are due to axonal packing rather than myelin levels, or perhaps other techniques used here are not sensitive to gender-related factors.

Through this analysis, the left and right uncinate fasciculus showed unique findings compared to other regions. The uncinate fasciculus was the only region to exhibit age-related changes in *g*-ratio, and was the only region to exhibit age-by-gender interactions in MD. These findings suggest that the uncinate is undergoing unique development during late childhood and adolescence, and this development is unique between boys and girls. This hypothesis is supported by the prolonged developmental period of the uncinate observed in previous studies (Krogsrud et al., 2016; Lebel, Walker, et al., 2008). As connections between prefrontal and temporal cortices are involved in many sophisticated cognitive skills that are refined during adolescence, the uncinate fasciculus is likely an important structure to consider in future developmental studies of late childhood and adolescence.

This study has several limitations. First, not everyone provided longitudinal data, and younger participants contributed fewer longitudinal data points than older participants. This age imbalance may have contributed to our observation of linear relationships between measures and age, rather than the nonlinear trajectories typically seen earlier in development. An incomplete longitudinal sample also decreases our statistical power. Future studies with complete longitudinal data may be better able to elucidate the specific maturation trajectories of qihMT and *g*-ratio. Future studies with more time points for each individual may also consider including random slopes per subject in their mixed models approach to account for individual differences in white matter development trajectories. Additionally, information regarding pubertal stage was not collected, even though it may influence white matter development (Genc, Seal, et al., 2017; Menzies, Goddings, Whitaker, Blakemore, & Viner, 2015). Furthermore, while VF_m and qihMT are much more specific to myelin than DTI measures, VF_m may also be affected by unwanted factors such as magnetization transfer, inflammation, or field inhomogeneities (Deoni et al., 2008; Lenz, Klarhofer, & Scheffler, 2010; Zhang, Kolind, Laule, & MacKay, 2015). ihMT may be affected by the orientation of underlying tissue, or other lipid membranes such as those found in neurons and glia (Manning et al., 2017).

5 | CONCLUSIONS

We have shown that changes in VF_m, NDI, FA, and MD and are widespread throughout childhood and adolescence, while no age-related trends were detected for ODI, qihMT, and *g*-ratio, with the exception of *g*-ratio changes in the bilateral uncinate fasciculus. Age effects for measures varied regionally, but can be grouped to highlight clusters of tracts developing similarly in our sample. A network of right hemisphere tracts showed age effects for NDI only, while most other major white matter tracts showed relationships with age for NDI and VF_m. Finally, the bilateral uncinate fasciculi showed age effects for *g*-ratio alongside NDI and VF_m, suggesting unique development of white matter microstructure in these frontotemporal connections. Gender effects were found for FA in the left cingulum only, and an age-by-gender interaction was observed for MD in the left uncinate fasciculus. This implies few gender-related differences in adolescent development, and suggests DTI measures may assess gender-related aspects of white matter microstructure that are bypassed by the more specific measures applied here. VF_m, qihMT, NDI, and *g*-ratio findings here suggest that ongoing myelination is driven by volume increases rather changes in membrane count, and that myelin volume increases occur in similar proportion to axon volume changes (i.e., *g*-ratio trends with age were mostly absent). It is only by combining these four microstructurally-sensitive measures that we may comment so specifically on myelin development in late childhood and adolescence. These findings elaborate our understanding of white matter development postinfancy, and provide a baseline by which to compare developmental disorders and evaluate response to intervention. A greater appreciation for the microstructural nuances of white matter maturation will help future studies to investigate the biological causes driving behavioral and developmental disorders.

ACKNOWLEDGMENTS

This project was supported by the Natural Science and Engineering Research Council (NSERC). Salary funding is provided by NSERC (BG) and the Canadian Institutes of Health Research (CL).

CONFLICT OF INTEREST

RML is an employee of General Electric Healthcare.

DATA AVAILABILITY STATEMENT

Data used in this study is available upon request to the principal investigator.

ORCID

Catherine Lebel https://orcid.org/0000-0002-0344-4032

REFERENCES

Avants, B. B., Tustison, N. J., Song, G., Cook, P. A., Klein, A., & Gee, J. C. (2011). A reproducible evaluation of ANTs similarity metric performance in brain image registration. *NeuroImage*, *54*(3), 2033–2044. https://doi.org/10.1016/j.neuroimage.2010.09.025

Beaulieu, C. (2002). The basis of anisotropic water diffusion in the nervous system—A technical review. *NMR in Biomedicine*, *15*, 435–455. https://doi.org/10.1002/nbm.782

Benes, F. M. (1989). Myelination of cortical-hippocampal relays during late adolescence. *Schizophrenia Bulletin*, *15*(4), 585–593.

Benjamini, Y., & Hochberg, Y. (1995). Controlling the false discovery rate: A practical and powerful approach to multiple testing. *Journal of the Royal Statistical Society*, *57*(1), 289–300.

Benjamini, Y., & Yekutieli, D. (2001). The control of the false discovery rate in multiple testing under dependency. *The Annals of Statistics*, *29*(4), 1165–1188.

Berry, I., Barker, G., Barkhof, F., Campi, A., Dousset, V., Franconi, J., … Tofts, P. S. (1999). A multicenter measurement of magnetization transfer ratio in normal white matter. *Journal of Magnetic Resonance Imaging*, *9*, 441–446.

Bonekamp, D., Nagae, L. M., Degaonkar, M., Matson, M., Abdalla, W. M., Barker, P. B., … Horska, A. (2007). Diffusion tensor imaging in children and adolescents: Reproducibility, hemispheric, and age-related differences. *NeuroImage*, *34*(2), 733–742. https://doi.org/10.1016/j.neuroimage.2006.09.020

Chang, Y. S., Owen, J. P., Pojman, N. J., Thieu, T., Bukshpun, P., Wakahiro, M. L., … Mukherjee, P. (2015). White matter changes of Neurite density and fiber orientation dispersion during human brain maturation. *PLoS One*, *10*(6), e0123656. https://doi.org/10.1371/journal.pone.0123656

Chen, Z., Zhang, H., Yushkevich, P. A., Liu, M., & Beaulieu, C. (2016). Maturation along white matter tracts in human brain using a diffusion tensor surface model tract-specific analysis. *Frontiers in Neuroanatomy*, *10*, 9. https://doi.org/10.3389/fnana.2016.00009

Dean, D. C., 3rd, O'Muircheartaigh, J., Dirks, H., Travers, B. G., Adluru, N., Alexander, A. L., & Deoni, S. C. (2016). Mapping an index of the myelin g-ratio in infants using magnetic resonance imaging. *NeuroImage*, *132*, 225–237. https://doi.org/10.1016/j.neuroimage.2016.02.040

Dean, D. C., 3rd, O'Muircheartaigh, J., Dirks, H., Waskiewicz, N., Lehman, K., Walker, L., … Deoni, S. C. (2015). Estimating the age of healthy infants from quantitative myelin water fraction maps. *Human Brain Mapping*, *36*(4), 1233–1244. https://doi.org/10.1002/hbm.22671

Deoni, S. C., Dean, D. C., 3rd, O'Muircheartaigh, J., Dirks, H., & Jerskey, B. A. (2012). Investigating white matter development in infancy and early childhood using myelin water faction and relaxation time mapping. *NeuroImage*, *63*(3), 1038–1053. https://doi.org/10.1016/j.neuroimage.2012.07.037

Deoni, S. C., Matthews, L., & Kolind, S. H. (2013). One component? Two components? Three? The effect of including a nonexchanging "free" water component in multicomponent driven equilibrium single pulse observation of T1 and T2. *Magnetic Resonance in Medicine*, *70*(1), 147–154. https://doi.org/10.1002/mrm.24429

Deoni, S. C., Mercure, E., Blasi, A., Gasston, D., Thomson, A., Johnson, M., … Murphy, D. G. (2011). Mapping infant brain myelination with magnetic resonance imaging. *The Journal of Neuroscience*, *31*(2), 784–791. https://doi.org/10.1523/JNEUROSCI.2106-10.2011

Deoni, S. C. L., Rutt, B. K., Arun, T., Pierpaoli, C., & Jones, D. K. (2008). Gleaning multicomponentT1andT2information from steady-state imaging data. *Magnetic Resonance in Medicine*, *60*(6), 1372–1387. https://doi.org/10.1002/mrm.21704

Eluvathingal, T. J., Hasan, K. M., Kramer, L., Fletcher, J. M., & Ewing-Cobbs, L. (2007). Quantitative diffusion tensor tractography of association and projection fibers in normally developing children and adolescents. *Cerebral Cortex*, *17*(12), 2760–2768. https://doi.org/10.1093/cercor/bhm003

Fields, R. D. (2008). White matter in learning, cognition and psychiatric disorders. *Trends in Neurosciences*, *31*(7), 361–370. https://doi.org/10.1016/j.tins.2008.04.001

Geeraert, B., Lebel, R. M., Mah, A. C., Deoni, S. C., Alsop, D. C., Varma, G., & Lebel, C. (2018). A comparison of inhomogeneous magnetization transfer, myelin volume fraction, and diffusion tensor imaging measures in healthy children. *NeuroImage*, *182*, 343–350. https://doi.org/10.1016/j.neuroimage.2017.09.019

Geeraert, B., Reynolds, J., & Lebel, C. (in press). Diffusion imaging perspectives on brain development in childhood and adolescence. In *Oxford handbook on developmental cognitive neuroscience*. Oxford University Press. https://doi.org/10.13140/RG.2.2.34652.23687

Genc, S., Malpas, C. B., Holland, S. K., Beare, R., & Silk, T. J. (2017). Neurite density index is sensitive to age related differences in the developing brain. *NeuroImage*, *148*, 373–380. https://doi.org/10.1016/j.neuroimage.2017.01.023

Genc, S., Seal, M. L., Dhollander, T., Malpas, C. B., Hazell, P., & Silk, T. J. (2017). White matter alterations at pubertal onset. *NeuroImage*, *156*, 286–292. https://doi.org/10.1016/j.neuroimage.2017.05.017

Giorgio, A., Watkins, K. E., Chadwick, M., James, S., Winmill, L., Douaud, G., … James, A. C. (2010). Longitudinal changes in grey and white matter during adolescence. *NeuroImage*, *49*(1), 94–103. https://doi.org/10.1016/j.neuroimage.2009.08.003

Helms, G., Dathe, H., Kallenberg, K., & Dechent, P. (2008). High-resolution maps of magnetization transfer with inherent correction for RF inhomogeneity and T1 relaxation obtained from 3D FLASH MRI. *Magnetic Resonance in Medicine*, *60*(6), 1396–1407. https://doi.org/10.1002/mrm.21732

Hurley, S. A., Mossahebi, P., Samsonov, A. A., Alexander, A. L., Deoni, S. C., Fisher, R., … Field, A. S. (2010). Multicomponent Relaxometry (mcDESPOT) in the shaking pup model of dysmyelination. *Proceedings of the International Society for Magnetic Resonance in Medicine*, *18*, 4516.

Jones, D. K., Knosche, T. R., & Turner, R. (2013). White matter integrity, fiber count, and other fallacies: The do's and don'ts of diffusion MRI. *NeuroImage*, *73*, 239–254. https://doi.org/10.1016/j.neuroimage.2012.06.081

Kass, R. E., & Raftery, A. E. (1995). Bayes factors. *Journal of the American Statistical Association*, *90*(430), 773–795.

Kolind, S., Matthews, L., Johansen-Berg, H., Leite, M. I., Williams, S. C., Deoni, S., & Palace, J. (2012). Myelin water imaging reflects clinical variability in multiple sclerosis. *NeuroImage*, *60*(1), 263–270. https://doi.org/10.1016/j.neuroimage.2011.11.070

Kolind, S., Seddigh, A., Combes, A., Russell-Schulz, B., Tam, R., Yogendrakumar, V., … Brex, P. A. (2015). Brain and cord myelin water imaging: A progressive multiple sclerosis biomarker. *NeuroImage: Clinical*, *9*, 574–580. https://doi.org/10.1016/j.nicl.2015.10.002

Krogsrud, S. K., Fjell, A. M., Tamnes, C. K., Grydeland, H., Mork, L., Due-Tonnessen, P., … Walhovd, K. B. (2016). Changes in white matter microstructure in the developing brain—A longitudinal diffusion tensor imaging study of children from 4 to 11years of age. *Neuroimage*, *124*(Pt A), 473–486. https://doi.org/10.1016/j.neuroimage.2015.09.017

Laule, C., & Moore, G. R. W. (2018). Myelin water imaging to detect demyelination and remyelination and its validation in pathology. *Brain Pathology*, *28*(5), 750–764. https://doi.org/10.1111/bpa.12645

Lebel, C., & Beaulieu, C. (2011). Longitudinal development of human brain wiring continues from childhood into adulthood. *The Journal of Neuroscience*, *31*(30), 10937–10947. https://doi.org/10.1523/JNEUROSCI.5302-10.2011

Lebel, C., Rasmussen, C., Wyper, K., Walker, L., Andrew, G., Yager, J., & Beaulieu, C. (2008). Brain diffusion abnormalities in children with fetal alcohol spectrum disorder. *Alcoholism, Clinical and Experimental Research*, *32*(10), 1732–1740. https://doi.org/10.1111/j.1530-0277.2008.00750.x

Lebel, C., Treit, S., & Beaulieu, C. (2017). A review of diffusion MRI of typical white matter development from early childhood to young adulthood. *NMR in Biomedicine*, *32*, e3778. https://doi.org/10.1002/nbm.3778

Lebel, C., Walker, L., Leemans, A., Phillips, L., & Beaulieu, C. (2008). Microstructural maturation of the human brain from childhood to adulthood. *NeuroImage*, *40*(3), 1044–1055. https://doi.org/10.1016/j.neuroimage.2007.12.053

Leemans, A., Jeurissen, B., Sijbers, J., & Jones, D. K. (2009). ExploreDTI: A graphical toolbox for processing, analyzing, and visualizing diffusion MR data. In: 17th Annual Meeting of Proceedings of International Society of Magnetic Resonance in Medicine, Hawaii, USA.

Lenz, C., Klarhofer, M., & Scheffler, K. (2010). Limitations of rapid myelin water quantification using 3D bSSFP. *MAGMA*, *23*(3), 139–151. https://doi.org/10.1007/s10334-010-0211-1

Mah, A., Geeraert, B., & Lebel, C. (2017). Detailing neuroanatomical development in late childhood and early adolescence using NODDI. *PLoS One*, *12*(8), e0182340. https://doi.org/10.1371/journal.pone.0182340

Manning, A. P., Chang, K. L., MacKay, A. L., & Michal, C. A. (2017). The physical mechanism of "inhomogeneous" magnetization transfer MRI. *Journal of Magnetic Resonance*, *274*, 125–136. https://doi.org/10.1016/j.jmr.2016.11.013

McHinda, S., Varma, G., Prevost, V. H., Le Troter, A., Rapacchi, S., Guye, M., … Girard, O. M. (2018). Whole brain inhomogeneous magnetization transfer (ihMT) imaging: Sensitivity enhancement within a steady-state gradient echo sequence. *Magnetic Resonance in Medicine*, *79*(5), 2607–2619. https://doi.org/10.1002/mrm.26907

Menzies, L., Goddings, A. L., Whitaker, K. J., Blakemore, S. J., & Viner, R. M. (2015). The effects of puberty on white matter development in boys. *Developmental Cognitive Neuroscience*, *11*, 116–128. https://doi.org/10.1016/j.dcn.2014.10.002

Moura, L. M., Kempton, M., Barker, G., Salum, G., Gadelha, A., Pan, P. M., … Jackowski, A. P. (2016). Age-effects in white matter using associated diffusion tensor imaging and magnetization transfer ratio during late childhood and early adolescence. *Magnetic Resonance Imaging*, *34*(4), 529–534. https://doi.org/10.1016/j.mri.2015.12.021

Muftuler, L. T., Davis, E. P., Buss, C., Solodkin, A., Su, M. Y., Head, K. M., … Sandman, C. A. (2012). Development of white matter pathways in typically developing preadolescent children. *Brain Research*, *1466*, 33–43. https://doi.org/10.1016/j.brainres.2012.05.035

Pangelinan, M. M., Leonard, G., Perron, M., Pike, G. B., Richer, L., Veillette, S., … Paus, T. (2016). Puberty and testosterone shape the corticospinal tract during male adolescence. *Brain Structure & Function*, *221*(2), 1083–1094. https://doi.org/10.1007/s00429-014-0956-9

Perrin, J. S., Leonard, G., Perron, M., Pike, G. B., Pitiot, A., Richer, L., … Paus, T. (2009). Sex differences in the growth of white matter during adolescence. *NeuroImage*, *45*(4), 1055–1066. https://doi.org/10.1016/j.neuroimage.2009.01.023

Prevost, V. H., Girard, O. M., McHinda, S., Varma, G., Alsop, D. C., & Duhamel, G. (2017). Optimization of inhomogeneous magnetization transfer (ihMT) MRI contrast for preclinical studies using dipolar relaxation time (T1D) filtering. *NMR in Biomedicine*, *30*(6), 1–13. https://doi.org/10.1002/nbm.3706

Rushton, W. A. H. (1951). A theory of the effects of fibre size in medullated nerve. *The Journal of Physiology*, *115*, 101–122.

Schmierer, K., Scaravilli, F., Altmann, D. R., Barker, G. J., & Miller, D. H. (2004). Magnetization transfer ratio and myelin in postmortem multiple sclerosis brain. *Annals of Neurology*, *56*(3), 407–415. https://doi.org/10.1002/ana.20202

Simmonds, D. J., Hallquist, M. N., Asato, M., & Luna, B. (2014). Developmental stages and sex differences of white matter and behavioral development through adolescence: A longitudinal diffusion tensor imaging (DTI) study. *NeuroImage*, *92*, 356–368. https://doi.org/10.1016/j.neuroimage.2013.12.044

Smith, S. M. (2002). Fast robust automated brain extraction. *Human Brain Mapping*, *17*(3), 143–155. https://doi.org/10.1002/hbm.10062

Stanisz, G. J., Webb, S., Munro, C. A., Pun, T., & Midha, R. (2004). MR properties of excised neural tissue following experimentally induced inflammation. *Magnetic Resonance in Medicine*, *51*(3), 473–479. https://doi.org/10.1002/mrm.20008

Stikov, N., Campbell, J. S., Stroh, T., Lavelee, M., Frey, S., Novek, J., … Pike, G. B. (2015). In vivo histology of the myelin g-ratio with magnetic resonance imaging. *NeuroImage*, *118*, 397–405. https://doi.org/10.1016/j.neuroimage.2015.05.023

Swanson, S. D., Malyarenko, D. I., Fabiilli, M. L., Welsh, R. C., Nielsen, J. F., & Srinivasan, A. (2017). Molecular, dynamic, and structural origin of inhomogeneous magnetization transfer in lipid membranes. *Magnetic Resonance in Medicine*, *77*(3), 1318–1328. https://doi.org/10.1002/mrm.26210

Tamnes, C. K., Ostby, Y., Walhovd, K. B., Westlye, L. T., Due-Tonnessen, P., & Fjell, A. M. (2010). Intellectual abilities and white matter microstructure in development: A diffusion tensor imaging study. *Human Brain Mapping*, *31*(10), 1609–1625. https://doi.org/10.1002/hbm.20962

Tamnes, C. K., Roalf, D. R., Goddings, A. L., & Lebel, C. (2017). Diffusion MRI of white matter microstructure development in childhood and adolescence: Methods, challenges and progress. *Developmental Cognitive Neuroscience*, *33*, 161–175. https://doi.org/10.1016/j.dcn.2017.12.002

Tax, C. M., Otte, W. M., Viergever, M. A., Dijkhuizen, R. M., & Leemans, A. (2015). REKINDLE: Robust extraction of kurtosis INDices with linear estimation. *Magnetic Resonance in Medicine*, *73*(2), 794–808. https://doi.org/10.1002/mrm.25165

Uda, S., Matsui, M., Tanaka, C., Uematsu, A., Miura, K., Kawana, I., & Noguchi, K. (2015). Normal development of human brain white matter from infancy to early adulthood: A diffusion tensor imaging study. *Developmental Neuroscience*, *37*(2), 182–194. https://doi.org/10.1159/000373885

Varma, G., Duhamel, G., de Bazelaire, C., & Alsop, D. C. (2015). Magnetization transfer from inhomogeneously broadened lines: A potential marker for myelin. *Magnetic Resonance in Medicine*, *73*(2), 614–622. https://doi.org/10.1002/mrm.25174

Wood, T. C., Simmons, C., Hurley, S. A., Vernon, A. C., Torres, J., Dell'Acqua, F., … Cash, D. (2016). Whole-brain ex-vivo quantitative MRI of the cuprizone mouse model. *PeerJ*, *4*, e2632. https://doi.org/10.7717/peerj.2632

Yakovlev, P. I., & Lecours, A.-R. (1967). The myelogenetic cycles of regional maturation of the brain. In Minkowski, A. (Ed.). *Regional Development of the Brainin Early Life* (pp. 3–70). Oxford: Blackwell.

Zaiss, M., Xu, J., Goerke, S., Khan, I. S., Singer, R. J., Gore, J. C., … Bachert, P. (2014). Inverse Z-spectrum analysis for spillover-, MT-, and T1 -corrected steady-state pulsed CEST-MRI—Application to pH-weighted MRI of acute stroke. *NMR in Biomedicine*, *27*(3), 240–252. https://doi.org/10.1002/nbm.3054

Zhang, H., Schneider, T., Wheeler-Kingshott, C. A., & Alexander, D. C. (2012). NODDI: Practical in vivo neurite orientation dispersion and density imaging of the human brain. *NeuroImage*, *61*(4), 1000–1016. https://doi.org/10.1016/j.neuroimage.2012.03.072

Zhang, J., Kolind, S. H., Laule, C., & MacKay, A. L. (2015). How does magnetization transfer influence mcDESPOT results? *Magnetic Resonance in Medicine*, *74*(5), 1327–1335. https://doi.org/10.1002/mrm.25520

SUPPORTING INFORMATION

Additional supporting information may be found online in the Supporting Information section at the end of this article.

How to cite this article: Geeraert BL, Lebel RM, Lebel C. A multiparametric analysis of white matter maturation during late childhood and adolescence. *Hum Brain Mapp*. 2019;1–12. https://doi.org/10.1002/hbm.24706